Prediction of dryout type critical heat flux and relevant thermal-hydraulic issues

OKAWA Tomio

Department of Mechanical Engineering, Graduate School of Engineering, Osaka University; 2-1, Yamadaoka, Suita-shi, Osaka 565-0871, Japan (t-okawa@mech.eng.osaka-u.ac.jp)

Abstract: Liquid film dryout in annular two-phase flow is a crucial problem to ensure the safety of nuclear power plants since it is a main triggering mechanism of the critical heat flux condition in high-quality flow boiling encountered in nuclear reactor core. This article presents the outline of the prediction methods of the wall heat flux at which the liquid film dryout takes place. Effects of additional factors related to the dryout are also discussed. The factors discussed herein include the spacer effect on the droplet deposition, the effect of flow oscillation on the critical heat flux and the droplet entrainment induced by the drop impact.
Keyword: liquid film dryout; annular flow model; spacer effect; flow oscillation; secondary entrainment

1 Introduction

Critical heat flux in forced-convective flow boiling is one of the most important design parameters of nuclear power plants, since the fuel temperature increases rapidly due to a sudden reduction of heat transfer coefficient if the critical heat flux condition is reached. First, we consider the following simple situation: flow channel is a round tube, a working fluid is water, and the channel wall is heated uniformly. In this case, the critical heat flux can be expressed as a function of several parameters including pressure, tube diameter, heated length, flow rate, and inlet temperature. Here, the effects of several additional factors such as the wettability and the roughness of the heated surface and the dissolved gas in water are assumed to be insignificant for simplicity. Since the critical heat flux is a function of a reasonably small number of parameters and a number of experimental data are available, many correlations were developed so far[1–4]. As one of the best correlations, Katto and Ohno's correlation is shown below:

$$\frac{q_c}{G\Delta h_v} = X\left(1 + K\frac{\Delta h_s}{\Delta h_v}\right) \tag{1}$$

where q_c is the critical heat flux, G is the mass flux, Δh_v is the latent heat of vaporization, and Δh_s is the inlet subcooling; X and K are rather complicated functions of the following three dimensionless groups $L^* = L/D$, $R^* = \rho_g/\rho_l$, and $W^* = \sigma\rho_l/G^2L$; here, L is the heated length, D is the tube diameter, ρ is the density, σ is the surface tension, and the subscripts g and l denote gas and liquid phases, respectively. For example, under the conditions of low pressure, low mass flux and long tube, X and K are calculated by

$$X = 0.34W^{*0.043}/L^* \tag{2}$$

$$K = 0.77/W^{*0.043} \tag{3}$$

This kind of correlations is definitely useful for prompt estimation of the critical heat flux. However, even if the correlation is represented in a dimensionless form, it should still be regarded as an empirical correlation since it is not based on physical mechanisms to induce the critical heat flux condition. Therefore, great care is indispensable to use the correlations outside the range which the base experimental data of individual correlations cover. In addition, if the heat flux distribution is non-uniform or the flow rate is not constant, it is generally impossible to define the situation with a small number of parameters. It is considered that these difficulties of the empirical methods as well as scientific interests led to developments of more mechanistically- or phenomenologically-based methods for the critical heat flux.

The mechanisms leading to the critical heat flux condition in flow boiling can roughly be divided into the two types: the departure from nucleate boiling (DNB) and the liquid film dryout. Although the DNB is not the main topic of this article, it has a close relation to the transition from nucleate boiling to film

Received date: August 3, 2010

boiling observed in heat-flux-controlled pool boiling experiments. In high-vapor-quality flow boiling, the critical heat flux condition is reached at the lower heat flux since the flow pattern transition to the annular two-phase flow takes place in a boiling channel. In this case, the channel wall is exposed to the vapor phase when the liquid film is depleted, and the wall temperature rises sharply due to the sudden deterioration of the heat transfer coefficient. Hewitt, *et al*. would be the first to provide clear experimental evidence that the onset of critical heat flux condition in annular two-phase flow regime corresponds closely to the depletion of the liquid film. They performed simultaneous measurements of the film flow rate and the wall temperature in uniformly heated boiling channels to show that the critical heat flux at which the temperature excursion took place was very close to the heat flux at which the local film flow rate at the channel exit became zero[5,6].

The understanding of the situation at the onset of critical heat flux condition led to a development of the annular flow model that enabled more mechanistic prediction of the critical heat flux caused by the liquid film dryout[7]. The annular flow model overcame some of the difficulties associated with fully-empirical CHF correlations. It should however be noted that a number of simplifications and empirical constants are needed to calculate the axial distribution of the film flow rate in a boiling channel. Therefore, empiricism still remains even in the annular flow model. In the present article, the prediction of CHF using the annular flow model is outlined, and then thermal- hydraulic issues regarding its general validity are discussed.

2 Prediction of dryout type CHF

2.1 Annular flow model

A distinct feature of annular two-phase flow is that liquid phase flows partly as entrained droplets in high-velocity gas core and partly as a liquid film moving along a channel wall. Entrainment fraction is hence used as the term to express the ratio of the droplet flow rate to the total liquid flow rate. In adiabatic annular flow, the entrainment fraction near the mixing section is dependent on the method to mix the gas and liquid phases, but it reaches a quasi-equilibrium state sufficiently downstream from the mixing section[8]. This experimental evidence indicates that mass transfers are present between the droplets and the liquid film in annular two-phase flow. Different terminologies are used to express the mass transfer process from the droplets to the liquid film and that in the opposite direction. The former is the droplet deposition and the latter is the droplet entrainment. In diabatic annular flow, it may further be assumed that the wall heat flux is spent for the vaporization of the liquid film. Therefore, variation of the film flow rate in the axial direction is expressed by

$$\frac{dG_f}{dz} = \frac{4}{D}(m_d - m_e - m_v) \tag{4}$$

where G_f is the mass flux of a liquid film, z is the axial coordinate, D is the tube diameter, m_d is the deposition rate of droplets, m_e is the entrainment rate of droplets, and m_v is the vaporization rate. Equation 4 is a first-order ordinary differential equation. Therefore, if it is integrated numerically, axial distribution of G_f can be calculated without difficulty. Since m_v is a monotonically increasing function of the wall heat flux q_w, G_f decreases with an increase in q_w. The value of q_w at which the minimum value of G_f within a boiling channel is small enough can be regarded as the critical heat flux.

In Eq. (4), we can see several advantages of the annular flow model over the fully-empirical correlations. First, the annular flow model requires no special treatments for axially non-uniform heating. Since it predicts the axial distribution of G_f, not only the critical heat flux but also the dryout point is readily calculated. Second, Eq. (4) can be extended for the dryout in a transient state[9] as well as the situation in which multiple liquid films are present[10]. Therefore, the annular flow model is applicable to more complicated situations such as the transient dryout and the liquid film dryout in annuli and rod bundles. One can expect that these features are particularly advantageous in the application to the prediction of the critical heat flux in nuclear reactor core.

2.2 Correlations

To perform the integration of Eq. (4), appropriate correlations are necessary to evaluate the mass

transfer rates and to specify boundary conditions. Due to empirical constants included in the correlations, general validity of the calculated CHF values suffers certain deterioration. Since numerous correlations were developed so far, the correlations used in author's work[11] are mainly discussed in this section.

2.2.1 Mass transfer rates

First, the methods to evaluate m_d, m_e and m_v in Eq. (4) are discussed. In order to express m_d with simple equations, it is generally assumed that m_d is proportional to the droplet concentration in the gas core C:

$$m_d = k_d C \tag{5}$$

where k_d is a droplet transfer coefficient having the units of velocity. If the liquid film is sufficiently thin and the droplet velocity relative to the gas phase is neglected, C is calculated by

$$C \approx \rho_g G_d / G_g \tag{6}$$

where ρ is the density, G is the mass flux, and the subscripts g and d denote the gas phase and droplets, respectively. Accurate evaluation of k_d is a particularly important step in predicting the CHF using the annular flow model. It is known that k_d is dependent on various parameters such as the flow rate of gas phase[12] and the droplet concentration in the gas core[13]. It was also reported that some detailed experimental setup has an additional influence on k_d[14,15]. For better prediction of k_d, Okawa, *et al.*[11] used the following two correlations depending on the flow conditions.

$$k_d \sqrt{\frac{\rho_g D}{\sigma}} = 0.0632 \left(\frac{C}{\rho_g} \right)^{-0.5} \tag{7}$$

$$\frac{\rho_g k_d}{G_g} = 0.009 \left(\frac{C}{\rho_g} \right)^{-0.5} \left(\frac{G_g D}{\mu_g} \right)^{-0.2} Pr_g^{-2/3} \tag{8}$$

where μ is the viscosity and Pr is the Prandtl number. Equation 7 is based on the experimental data for various fluids including water compiled by Govan, *et al.*[13] and Eq. (8) was developed by Sugawara using the data for steam-water annular flow[16]. In the earlier stage, the correlation was developed based entirely on dimensional analysis. In recent studies, detailed numerical simulations were carried out to elucidate the mechanisms to determine the dependence of k_d on various parameters[17–19]. For example, Yamamoto and Okawa[19] conducted particle tracking simulations to show that modification of turbulent flow field in the gas core plays a significant role in causing a reduction of k_d with an increase in C.

Direct measurement of the entrainment rate is very difficult. In the determination of entrainment rate, it is usually assumed that the entrainment rate is equal to the deposition rate in the equilibrium region of adiabatic annular flow. Therefore, the data of m_d obtained in the equilibrium region may be used to develop the correlation for m_e[15]. In the alternative method, the data of the entrainment fraction in the equilibrium region E_{eq} are used. Since $G_d = E_{eq} G_l$,, the assumption of $m_e = m_d$ leads to

$$m_e = k_d \rho_g E_{eq} G_l / G_g \tag{9}$$

Okawa, *et al.*[11,20] further assumed that the droplet entrainment is enhanced by the interfacial shear force acting on a liquid film while suppressed by the surface tension force acting on it, and introduced the following dimensionless number defined as the ratio of the two forces.

$$\pi_e = \frac{f_i G_g^2 \delta}{\rho_g \sigma} \tag{10}$$

where f_i is the interfacial friction factor and δ is the film thickness. They showed that the data of E_{eq} reported in various sources are collapsed satisfactorily well if the following functional form is assumed for m_e.

$$m_e = k_e \rho_l \pi_e^n \tag{11}$$

where the proportionality factor k_e and the exponent n are the model constants and their values are dependent on the range of π_e[11]. Okawa, *et al.*[11] further included the contribution of the boiling that would take place in a liquid film in diabatic annular flow. The correlation developed by Ueda, *et al.*[21] was used for this purpose. The correlation is based on the experiments on the droplet entrainment from a freely falling liquid film on vertical heated tubes, in which the shear force acting on a liquid film may be

neglected. It should however be noted that there would be a controversy whether or not the results for a freely falling film can be applied directly to a liquid film in annular two-phase flow.

It is considered that gas and liquid phases are nearly saturated in annular two-phase flow. It would be fair to assume that all the heat is spent for the vaporization of a liquid film.

$$m_v = q_w / \Delta h_v \tag{12}$$

where q_w is the heat flux.

2.2.2 Boundary conditions

To specify the upstream boundary condition of the integration, correlations are needed for the transition to annular flow and the entrainment fraction at the transition point. These correlations are particularly important for short tubes, in which the effect of the inlet condition tends to remain even at the channel exit[22]. Although many methods are available for the transition, one of the best ones would be that proposed by Wallis[23].

$$x_t = \frac{0.6 + 0.4\sqrt{gD(\rho_l - \rho_g)\rho_l}/G}{0.6 + \sqrt{\rho_l / \rho_g}} \tag{13}$$

where x_t is the quality at the transition and g is the gravitational acceleration. Since the entrainment fraction is usually measured in the equilibrium region of adiabatic annular flow, experimental information for the entrainment fraction at the transition to annular flow E_t is scarce. It may hence be most presumable to assume that the hydrodynamic equilibrium ($m_d = m_e$) is established promptly at the transition point to calculate E_t.

Circumferential distribution of a liquid film would not be perfectly uniform even in a round tube, and local instantaneous film flow rate would not be constant even in a steady state due to the presence of interfacial waves such as ripple and disturbance waves. Therefore, in a strict sense, local instantaneous film flow rate can be zero to cause temperature excursion before the cross-sectional and time averaged film flow rate that is the flow rate calculated by the annular flow model becomes zero. In addition, a certain amount of liquid is needed to cover the heated surface completely. These lead to the concept of critical film flow rate at which a sudden increase in the wall temperature occurs. Okawa, *et al*.[11] modified the correlation by Ueda and Isayama[24] to evaluate the critical film flow rate. In many conditions of interest, however, the CHF value calculated by the annular flow model is not dependent significantly on the critical film flow rate[22]. Therefore, the use of the simplest assumption that the complete depletion of a liquid film corresponds to sudden deterioration of heat transfer would also be recommended. However, the critical heat flux is sometimes overestimated even if the predictions of the film flow rate at the heat fluxes less than CHF are satisfactory[23]. Such discrepancies may be attributed to present insufficient understanding of the situation at the onset of critical heat flux condition.

2.3 Comparisons with experimental data

The annular flow model outlined in the previous section was used to calculate the dryout type critical heat flux in uniformly-heated round tubes. The results are depicted in Fig. 1[11]. It can be seen that the calculated CHFs are in fairly good agreements with experimental data (standard deviation is 0.128 for 1926 data). It was also demonstrated that the predictive performance is not deteriorated even for axially non-uniform heating and non-circular channels. In the case of thin rectangular channels, however, the present model tended to overestimate the critical heat flux. Accumulation of the liquid film at the corner sections was considered to be a main cause of the discrepancy.

In the calculation of CHF using the annular flow model, appropriate correlations should be prepared for extremely complex processes such as the deposition and entrainment of droplets. Evidently, further experimental and numerical studies are necessary to improve the accuracy and reliability of each correlation. However, all the correlations included in the present model were derived from the experimental data of the film flow rate and droplet flow rate in adiabatic and diabatic two-phase flows. At least, the model does not include the arbitrary constants that should be adjusted from the comparisons of the calculated and measured critical heat fluxes. Nonetheless, fairly good agreements

could be achieved as demonstrated in Fig. 1. It is considered that the annular flow model is a powerful tool to predict the dryout type critical heat flux.

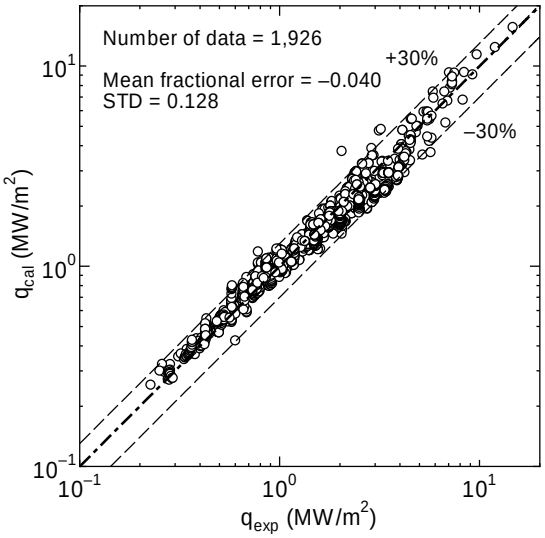

Fig. 1 Comparisons between measured and calculated dryout-type critical heat fluxes in uniformly heated vertical round tubes[11].

3 Relevant thermal-hydraulic issues

To apply the annular flow model to the prediction of the CHF in nuclear reactor core and more complicated situations, additional issues frequently arise. Such issues addressed in author's laboratory are discussed in what follows.

3.1 Spacer effect

In the fuel assemblies in nuclear reactor core, the rod spacing devices called spacer are used to maintain the configuration of fuel rods. Although the primary purpose of the spacer is to keep the arrangement of fuel rods, it is known that it enhances the critical heat flux[26,27]. The spacer effect on the critical heat flux can be attributed to the enhancement of droplet deposition. In annular two-phase flow, the droplet paths are nearly parallel to the channel wall. Slight deviation from the ideal path causes the droplet deposition on a liquid film. The spacer can be regarded as the flow obstacle placed in a boiling channel. It may be expected that the droplet paths are deviated significantly from the ideal ones and many droplets are deposited on a liquid film around the spacer.

In order to elucidate the detailed mechanisms of the deposition enhancement, a series of air-water experiments were carried out[28–30]. The test sections are shown schematically in Fig. 2[30]. The air-water annular flow entered the test section from its bottom. The test section was a 5 mm diameter vertical round tube. The whole of the liquid film was extracted together with a small amount of air at the first extraction unit, in which the tube wall was made of porous material. Since the remaining droplets were re-deposited onto the tube wall, a new liquid film was build up between the first and second extraction units. The new liquid film was extracted at the second film extraction unit to calculate the deposition rate of droplets within the re-deposition section. Five small tubes of 20 mm in length were placed concentrically in the test section to explore the obstacle effect on the droplet deposition. The five obstacles had different inner and outer diameters; their blockage ratios were within 0.12–0.40. In many models for the spacer effect, it is hypothesized that the deposition enhancement is mainly caused downstream of the flow obstacle due to turbulence augmentation, drift flow, run-off effect, *etc*. It was however speculated that the deposition enhancement occurs not only downstream but also at the inlet of the obstacle section. In the present experiment, the obstacles were placed at the three axial locations as depicted in Fig. 2. It was supposed that the film flow rate measured at the second film extraction unit reflects no obstacle effect in the first configuration, includes the deposition enhancement at the inlet of the obstacle section in the second configuration, and the whole of the obstacle effect in the third configuration.

As typical experimental data, the film flow rates relative to the total liquid flow rates measured for Type-R obstacle (D_i = 2.0mm, D_o = 3.0mm, β_b = 0.20) and Type-D1 obstacle (D_i = 1.0mm, D_o = 2.5mm, β_b = 0.21) are depicted in Fig. 3; here, D_i and D_o are the inner and outer diameters of the obstacle tube and β_b is the blockage ratio. It can be seen that the film flow rate was significantly greater downstream of the obstacles than upstream in all the experimental conditions. Another important observation in Fig. 3 is that a noticeable increase in the film flow rate already took place at the middle of the flow obstacles. These results clearly indicate that the droplet deposition is enhanced significantly by the flow obstacle, and that the deposition enhancement occurs not only

downstream but also at the inlet of the obstacle section.

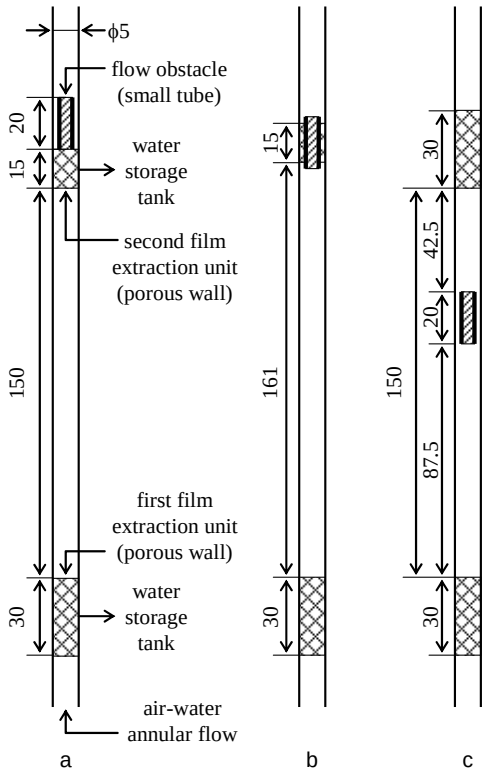

Fig. 2 Schematic diagram of the deposition rate measuring section; a new liquid film is extracted (a) upstream, (b) at the middle, and (c) downstream of a flow obstacle[30]. (unit: mm)

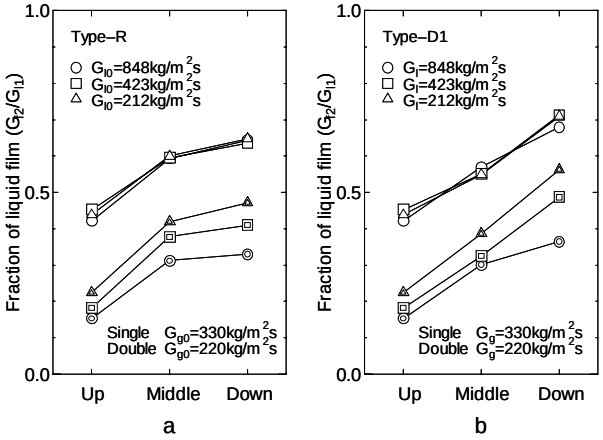

Fig. 3 Fractional flow rates of liquid film at the second film extraction unit; the liquid film was extracted (Up) upstream, (Middle) at the middle, and (Down) downstream of the small tubular flow obstacles; (a) Type-R obstacle and (b) Type-D1 obstacle[30].

Detailed analysis showed that the deposition enhancement at the inlet became noticeable with an increase in the blockage ratio and a decrease in the obstacle diameter. The number of the droplets impinging on the front face of the obstacle would roughly be proportional to the cross-sectional area of the obstacle and the drift flow formed at the inlet section would tend to direct toward the channel wall for small-diameter tubes. It was therefore supposed that part of the droplets impinged on the obstacle, and then they were carried to the channel wall by the drift flow to contribute to the deposition enhancement. It was also shown that the deposition enhancement downstream of the obstacle was significant when the wall thickness of the obstacle was large. It was speculated that the size of the turbulent eddy formed behind the obstacle was influential in the deposition enhancement observed downstream of the obstacle.

Based on the results of air-water experiments, Okawa, *et al*. developed an empirical correlation and a mechanistic model for the obstacle-induced deposition enhancement[30,31]. The empirical correlation is

$$m_d = \frac{DG_{d1}}{4z_d}\left[1-\exp\left\{-\frac{4\rho_g(k_d z_d + k_{ds} z_{ds})}{G_g D}\right\}\right] \quad (14)$$

where G_{d1} is the droplet flow rate at the inlet of the obstacle section and z_d is the deposition length; $k_{ds}z_{ds}$ is the term to express the obstacle effect and expressed by

$$k_{ds} z_{ds} = 5.2\beta_b^{0.9}\beta_d^{-1.1}\left(\frac{\rho_g D}{\sigma}\right)^{-0.5} D \quad (15)$$

where β_d is the ratio of the mean obstacle diameter to the channel diameter. The mechanistic model only accounts for the deposition enhancement at the inlet and given by

$$m_d = \frac{DG_{d1}}{4z_d}\left[1-(1-\beta_s)\exp\left(-\frac{4\rho_g k_d z_d}{G_g D}\right)\right] \quad (16)$$

where β_s is the area ratio of the outer region beyond the stagnation line in the front face of the obstacle to the channel cross-section. Although these correlation and model were developed solely based on the air-water data, the deposition enhancement in steam-water annular flow was also predicted satisfactorily well, as demonstrated in Fig. 4[31]. It should be noted that the present correlation and model would not be applicable to intricately-shaped

spacers used in the nuclear reactor core. It is however expected that they provide conservative estimation of the spacer effect and can be used as the base of more sophisticated methods.

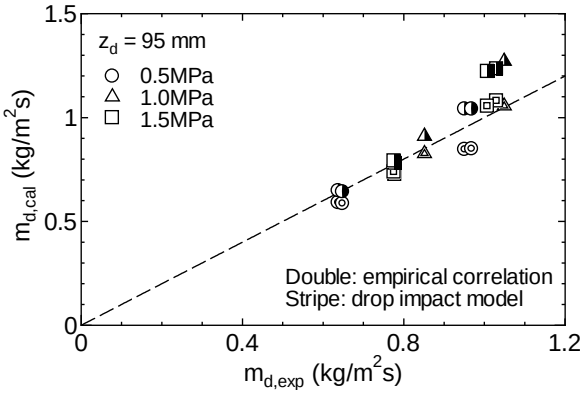

Fig. 4 Comparisons of calculated deposition rate of droplets with experimental data for steam-water annular flow in the channel containing a tubular flow obstacle[31].

3.2 Effect of flow oscillation

Since an increase in the core power density is one of the most promising ways to further improve the economic efficiency, high-power-density core is adopted in many advanced nuclear reactors. It is however known that an increase in the power density commonly leads to the reduction of the margin to the onset of unanticipated flow instability in boiling two-phase flow systems[32]. Therefore, to ensure the safety of the advanced nuclear reactors, a satisfactorily reliable method is needed to predict the critical heat flux even under the flow oscillation conditions as well as in the steady states.

We consider a rather simple situation in which the test section is a uniformly heated round tube and the inlet mass flux G is oscillated sinusoidally, as illustrated in Fig. 5.

$$G = G_{AVE} + \Delta G \sin\left(\frac{2\pi}{t_{OSC}} t\right) \tag{17}$$

where t is the time, G_{AVE} is the time-averaged inlet mass flux, ΔG is the oscillation amplitude, and t_{OSC} is the oscillation period. The minimum inlet mass flux G_{MIN} is equal to $G_{AVE} - \Delta G$. It is expected that, if the heat flux q_w is increased gradually, the first instantaneous dryout takes place at the channel exit when the fluid corresponding to G_{MIN} arrives at the channel exit. If the heated length L is short or the oscillation period t_{OSC} is long, the flow oscillation at the inlet would directly affect the dryout at the channel exit. In this case, the critical heat flux under the oscillatory condition q_{OSC} would be equal to q_{MIN} that is the critical heat flux in the steady state of $G = G_{MIN}$. Whilst, for sufficiently long L or sufficiently short t_{OSC}, the situation at the channel exit would not be influenced by the oscillation of the inlet mass flux. In this case, q_{OSC} would be equal to q_{AVE} that is the critical heat flux in the steady state of $G = G_{AVE}$. In view of these, Okawa, *et al.*[33] introduced the dimensionless critical heat flux q^* defined by

$$q^* = \frac{q_{OSC} - q_{MIN}}{q_{AVE} - q_{MIN}} \tag{18}$$

The fluid velocity in the liquid film depends on the film thickness. For example, the liquid can move only slowly in a thin film due to significant influence of the wall shear stress. It is therefore expected that interaction takes place between the thin and thick film regions to cause liquid transport from the thick to thin film regions. Based on the velocity difference within the liquid film under the flow oscillation condition, the dimensionless heated length L^* was derived to characterize the degree of interaction.

$$L^* = \frac{2L\sqrt{\rho_l \rho_g}}{G_{AVE} t_{OSC}} \left(\frac{\Delta G}{G_{AVE}}\right)^{0.2} \tag{19}$$

The alternative form of L^* was also derived using a nonlinear wave theory[34,35]. It was expected that q^* is expressed as a monotonically increasing function of L^*.

To test the validity of the proposed theory and to determine the functional relation between q^* and L^*, numerical simulations using a one-dimensional three-fluid model were performed. The basic equations of the three-fluid model consist of the conservation equations of mass, momentum and energy for a liquid film, droplets and gas phase[16]. The mass conservation equation for a liquid film is

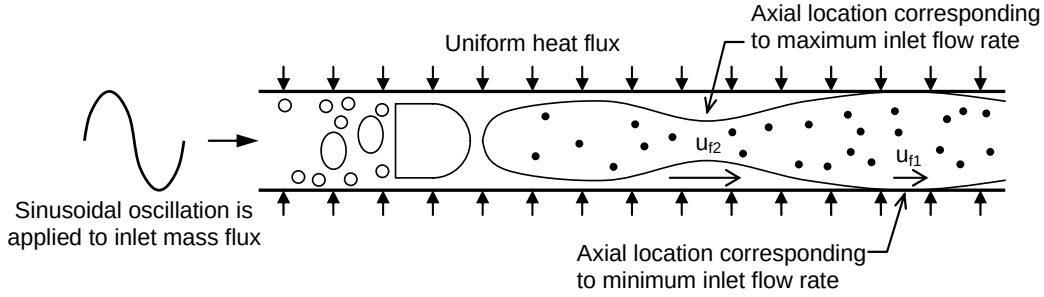

Fig. 5 Thermal-hydraulic condition supposed in a boiling channel under a flow oscillation condition[33].

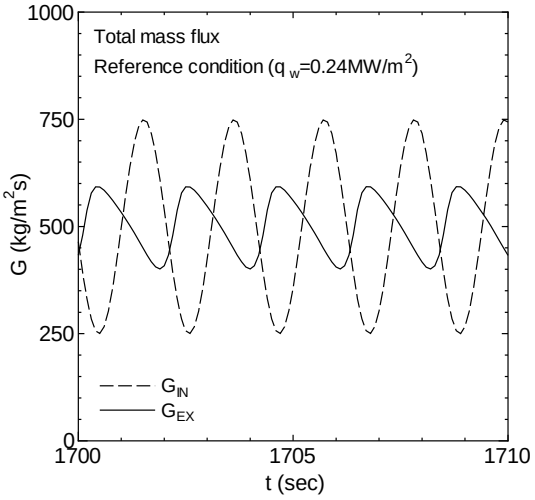

Fig. 6 Time variations of the inlet and outlet mass fluxes calculated using a one-dimensional three-fluid model[33].

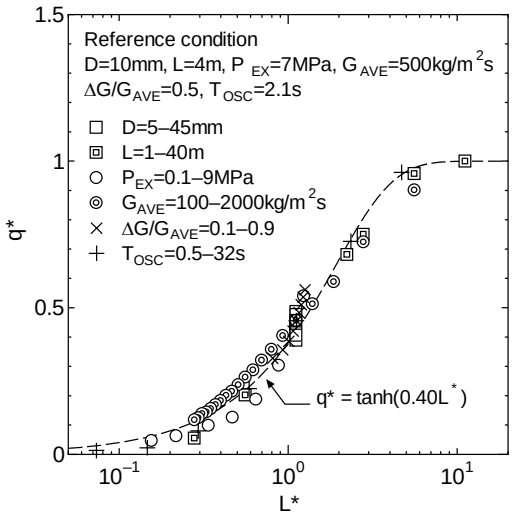

Fig. 7 Relation between the dimensionless heated length L^* and the dimensionless critical heat flux q^* in the numerical simulation[33].

reduced to the basic equation of the annular flow model in the steady state. The time variations of the mass fluxes at the inlet and outlet of the boiling channel are depicted in Fig. 6. The flow oscillation imposed at the inlet decayed noticeably at the outlet

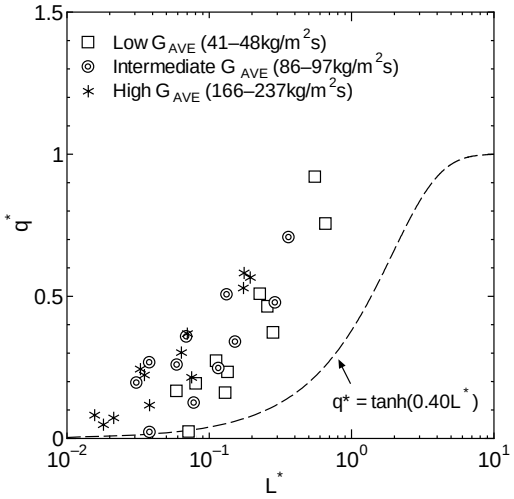

Fig. 8 Relation between the dimensionless heated length L^* and the dimensionless critical heat flux q^* in the experiment[33].

as expected in the proposed theory. The relation between L^* and q^* is explored in Fig. 7. It can be seen that the following simple function is satisfactory to express the relation between the two dimensionless numbers:

$$q^* = \tanh(0.4L^*) \tag{20}$$

Experimental measurements of the critical heat flux under flow oscillation conditions were conducted to test the validity of Eq. (20). The test section was a stainless steel tube of 12 mm in inner diameter and heated ohmically using a DC power supply; the heated length was 1.36 m. The test fluid was water and the experiments were conducted under the atmospheric pressure. To generate flow oscillation, electric power supplied to the circulation pump was oscillated sinusoidally. The experimental ranges of G_{AVE}, $\Delta G/G_{AVE}$ and t_{OSC} were 41–237 kg/m^{2}s, 0.25–0.84 and 2–20 s, respectively. The experimental results are shown in Fig. 8. As in the numerical simulation, q^* tended to increase with an increase in

L^*. However, Eq. (20) generally underestimates the experimental data. The liquid film in annular flow is covered by interfacial waves such as the ripple and disturbance waves[36,37]. In particular, the disturbance waves have a height several times the mean film thickness, move at a velocity greater than the mean film velocity, and retain their identity throughout the flow channel[38]. Their influence was however not taken into account in the numerical simulation. The discrepancy between the numerical and experimental results may hence be attributed to the axial liquid transport caused by the disturbance waves. Evidently, further studies are needed to elucidate the cause of the discrepancy. However, since the experimental data of the critical heat flux were generally greater than the values calculated by Eq. (20), the proposed correlation would be useful for the conservative estimation of the critical heat flux under flow oscillation conditions.

3.3 Secondary entrainment

In modeling the deposition rate and entrainment rate of droplets, it is commonly assumed that the droplets are absorbed in a liquid film after the collision and the interfacial shear force exerted by the high velocity gas core is the main cause of the droplet entrainment. It is however known that secondary droplets may be produced during the impact process[39]. The production process of the secondary droplets taken in author's laboratory is depicted in Fig. 9[40]. The sequential photographs clearly indicate that significant amount of secondary droplets can be produced during the impact process. In the case of the normal impingement of a water droplet on a thin water layer, the critical condition is expressed by[41]

$$\frac{\rho_l V^2 d}{\sigma} = 2100\left(\frac{\mu_l}{\sqrt{\rho_l \sigma d}}\right)^{0.4} \tag{21}$$

where V and d are the impact velocity and the droplet diameter, respectively. If the properties of the saturated water under the atmospheric pressure are substituted and the drop diameter is assumed to be 0.5 mm, the critical velocity calculated by the above equation is 4.8 m/s. The typical droplet velocity in annular flow is higher than this value, suggesting that the drop impact should also be taken into account as the mechanism of the droplet entrainment. The secondary entrainment is the term to express the droplet entrainment caused by the drop impact and has been concerned by many researchers in modeling the droplet transfer rates in annular two-phase flow.

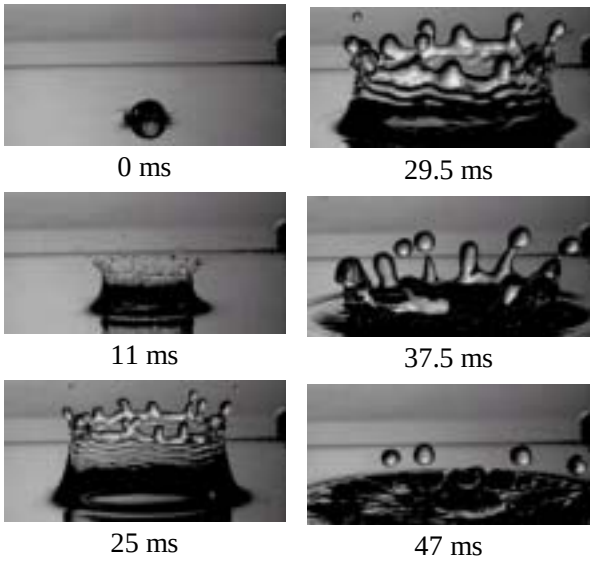

Fig. 9 Time-elapsed images of normal impact of a water droplet on a plane water surface (d = 4.1 mm, V = 3.6 m/s, h = 2 mm)[40].

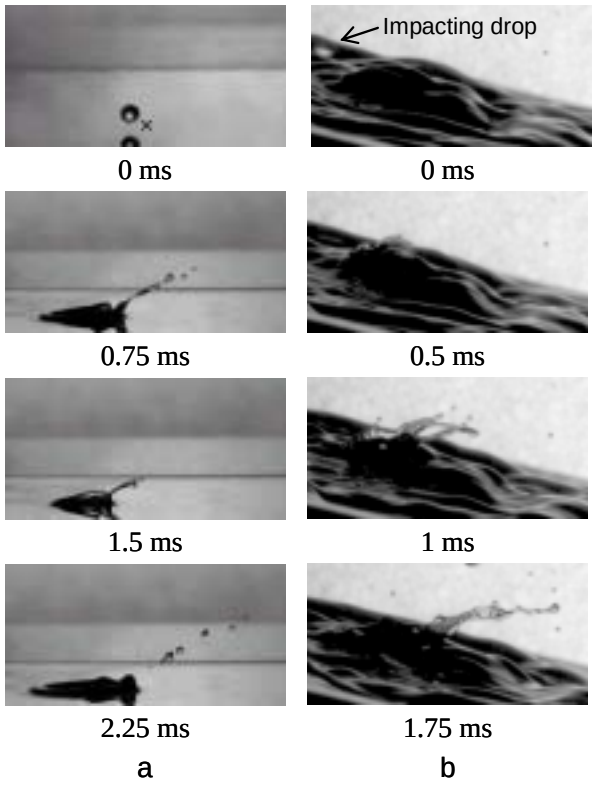

Fig. 10 Time-elapsed images of oblique impacts of single water droplets; (a) impact on a plane liquid layer (θ = 49º, *We* = 215), (b) impact on a falling liquid film (*We* = 379)[43].

One of the most distinct differences between available drop impact experiments and the situation

in annular flow is the impingement angle. In annular two-phase flow, the droplets impinge on a liquid film obliquely. If the radial droplet velocity is approximated by the friction velocity in turbulent pipe flow[42], the impingement angle from the film surface is only about 3º. In most experiments, however, droplets impinge on a target liquid layer normally with the impingement angle of 90º. The lack of detailed experimental information concerning the effect of impingement angle may be attributed to the technical difficulty to let droplets collide obliquely on a plane liquid surface.

To investigate the role of impingement angle, observations were made for oblique impacts of single water droplets[43,44]. The primary droplets were produced from a spray nozzle to let them collide obliquely. Typical observation results are depicted in Fig. 10. The primary droplets collided on a plane liquid layer and a freely falling liquid film in Figs. 10a and b, respectively. In both cases, secondary droplets were produced during the impact. At least in these cases, it is evident that the total volume of secondary droplets is not negligible comparing with that of primary droplet.

Let us return to Eq. (21). In oblique drop impact, not the total velocity component but the component normal to the surface may be of importance in determining the outcome of collision. If this is the case, V in the left-hand-side of Eq. (21) should be replaced by $V\sin\theta$ and the critical velocity is calculated about 100 m/s. The effect of θ on the deposition-splashing limit is explored in Fig. 11. Here, K is the impact K-number defined by $K = WeOh^{-0.4}$ and the total velocity component was used in calculating We. A plane liquid film was used as the target. It can be seen that the experimentally-determined limit agrees with Eq. (21) fairly well in moderately oblique impacts of $\theta > 30^\circ$. This indicates that the tangential as well as normal components were equally influential in determining the outcome of collision and was contrast to the drop impact on a solid surface in which the influencing factor is the momentum of the primary droplets in the direction normal to the surface and not the total momentum vector[45]. For very oblique impacts of $\theta < 30^\circ$,

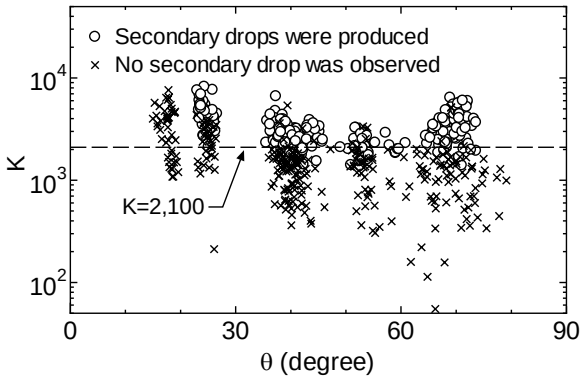

Fig. 11 Effect of the impingement angle on the deposition-splashing limit[44].

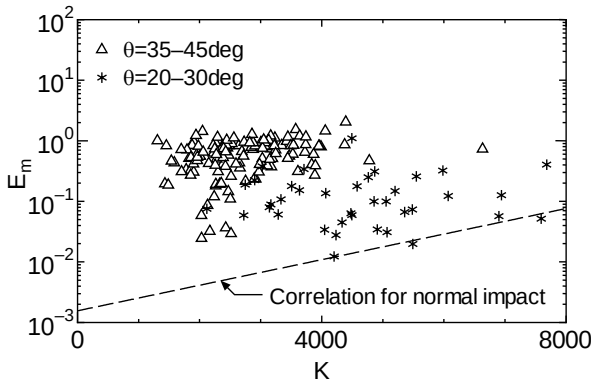

Fig. 12 Effect of the impingement angle on the total mass of secondary droplets[44].

however, θ had noticeable influence on the limit. The critical value of K increased to 3000–4000 at $\theta = 25^\circ$ and no splashing was observed for $\theta < 20^\circ$ under the experimental conditions tested. The experimental data of the amount of secondary droplets are shown in Fig. 12. Here, E_m denotes the mass ratio of the total secondary droplets to the primary droplet, and an empirical correlation for normal impact[40] is depicted for comparison. It might be surprising that the total amount of secondary droplets measured for moderately oblique impacts of $\theta = 35$–45° was about 100 times greater than that for normal impacts. It is considered that the remarkable increase of the secondary droplets can be attributed to the prow-like asymmetric interfacial structure developed during the impact (see Fig. 10). However, if the impingement angle is further reduced to 20–30º, the total amount of secondary droplets decreased significantly. In addition, when θ was less than 20º, production of secondary droplets was not observed even if K was greater than 7000. Okawa, *et al.* discussed that large portion of the kinetic energy of the primary droplet

was spent on the formation of liquid flow below the film surface in very oblique impacts[44]. These experimental results suggest that secondary entrainment plays a minor role in determining the mass transfer rates of droplets in annular two-phase flow.

4 Concluding remarks

The outline of the CHF prediction using the annular flow model and several relevant thermal-hydraulic issues were discussed. The annular flow model is a phenomenological model to calculate the axial evolution of the film flow rate in annular two-phase flow. It requires a number of correlations to evaluate various quantities that may affect the film flow rate. Since some quantities are determined through extremely complex rate processes, the use of the correlations containing empirical constants would be unavoidable. Therefore, the reliability of the calculated CHF values depends significantly on the accuracy of individual correlations. However, through mechanistically-based modifications, it can be applied to more complicated situations in which no experimental CHF data is available. This would be one of the most advantageous points over fully-empirical methods. The first-principle simulation of the whole thermal-hydraulic field in a boiling channel is still beyond the present computer power and numerical methods. The annular flow model and its extended versions such as the three-fluid model and subchannel analysis are definitely powerful tools to evaluate the critical heat flux particularly in nuclear reactor core. There is a substantial need to further improve these methods.

The relevant issues discussed herein are the spacer effect, the effect of flow oscillation on CHF and the secondary entrainment. It should however be noted that there are many other issues. Several examples are the cross flow: the fluid transport between subchannels in nuclear reactor core[46], the cold wall effect: the influence of non-heated wall on the spatial distribution of a liquid film[47], and peculiar behavior of CHF in bilaterally heated annuli[48]. The effects of rod bowing[49] and partial length rods[50] on behavior of droplets and a liquid film would also be interesting as well as important research topics.

Nomenclature

C	droplet concentration (kg/m^3)
D	tube diameter (m)
d	droplet diameter (m)
E	entrainment fraction (dimensionless)
f_i	interfacial friction factor (dimensionless)
G	mass flux (kg/m^{2}s)
E_m	mass ratio of the total secondary droplets to the primary droplet (dimensionless)
g	gravitational acceleration (m/s^2)
h	liquid layer thickness (m)
K	impact K-number (dimensionless)
k_d	droplet transfer coefficient (m/s)
k_e	proportionality factor in Eq. (11) (m/s)
L	heated length (m)
m_d	deposition transfer rate (kg/m^{2}s)
m_e	entrainment transfer rate (kg/m^{2}s)
m_v	vaporization transfer rate (kg/m^{2}s)
Oh	Ohnesorge number (dimensionless)
Pr	Prandtl number (dimensionless)
q	heat flux (W/m^2)
q_c	critical heat flux (W/m^2)
q_w	wall heat flux (W/m^2)
t	time (s)
t_{OSC}	oscillation frequency (s)
V	impact velocity (m/s)
We	Weber number (dimensionless)
x	vapor quality (dimensionless)
z_d	deposition length (m)

Greek symbols

β_b	blockage ratio (dimensionless)
β_d	diameter ratio (dimensionless)
β_s	area ratio of the outer region beyond the stagnation line in the front face of the obstacle to the channel cross-section (dimensionless)
ΔG	oscillation amplitude (kg/m^{2}s)
Δh_s	inlet subcooling (J/kg)
Δh_v	latent heat of vaporization (J/kg)
δ	film thickness (m)
μ	viscosity (Pa·s)
π_e	dimensionless number defined by Eq. (10) (dimensionless)
θ	impingement angle (dimensionless)
ρ	density (kg/m^3)
σ	surface tension (N/m)

Subscripts

1	inlet of deposition section
AVE	time average
d	droplet
eq	equilibrium
i	inside
f	liquid film
g	gas phase
l	liquid phase
MIN	minimum
OSC	oscillation
o	outside
s	obstacle effect
t	transition to annular flow

Superscript

*	dimensionless

References

[1] BERTOLETTI, S., GASPARI, G. P., LOMBARDI, C., PETERLONGO, G., SILVESTRI, M., TACCONI, F. A.: Heat transfer crisis with steam-water mixtures, Energia Nucleare, 12 (3), 121–172 (1965).

[2] TONG, L. S.: Critical heat fluxes in rod bundles, Proceedings of ASME Winter Meeting, Los Angeles, California, 31–46 (1969).

[3] BOWRING, R. W.: A simple but accurate round tube uniform heat flux dryout correlation over the pressure range 0.7–1.7 MN/m^2, AEEW-R789 (1972).

[4] KATTO, Y., OHNO, H.: An improved version of the generalized correlation of critical heat flux for the forced convective boiling in uniformly heated vertical tubes, International Journal of Heat and Mass Transfer, 27(9), 1641–1648 (1984).

[5] HEWITT, G. F., KEARSEY, H. A., LACEY, P. M. C., PULLING, D. J.: Burnout and nucleation in climbing film flow, AERE-R4374 (1963).

[6] HEWITT, G. F., KEARSEY, H. A., LACEY, P. M. C., PULLING, D. J.: Burnout and film flow in the evaporation of water in tubes, AERE-R4864 (1965).

[7] WHALLEY, P. B., HUTCHINSON, P., HEWITT, G. F.: The calculation of the critical heat flux in forced convection boiling, Proceedings of 5th International Heat Transfer Conference, Tokyo, Japan, Paper B6.11 (1974).

[8] HUTCHINSON, P., WHALLEY, P. B., HEWITT, G. F.: Transient flow redistribution in annular two-phase flow, International Journal of Multiphase Flow 1, 383–393 (1974).

[9] HEWITT, G. F., GOVAN, A.H.: Phenomenological modelling of non-equilibrium flows with phase change, International Journal of Heat and Mass Transfer 33 (2), 229–242 (1990).

[10] WHALLEY, P. B.: The calculation of dryout in a rod bundle, International Journal of Multiphase Flow 3 (6), 501–515 (1977).

[11] OKAWA, T., KOTANI, A., KATAOKA, I., NAITOH, M.: Prediction of the critical heat flux in annular regime in various vertical channels, Nuclear Engineering and Design 229, 233–236 (2004).

[12] MCCOY, D. D., HANRATTY, T. J.: Rate of deposition of droplets in annular two-phase flow, International Journal of Multiphase Flow 3 (4), 319–331 (1977).

[13] GOVAN, A. H., HEWITT, G. F., OWEN, D. G., BOTT, T. R.: An improved CHF modelling code, Proceedings of 2nd UK National Conference on Heat Transfer, Glasgow, UK, 33–48 (1988).

[14] COUSINS, L. B., HEWITT, G. F.: Liquid phase mass transfer in annular two-phase flow: droplet deposition and liquid entrainment, AERE-R5657 (1968).

[15] OKAWA, T., KATAOKA, I.: Correlations for the mass transfer rate of droplets in vertical upward annular flow, International Journal of Heat and Mass Transfer 48 (23–24), 4766–4778 (2005).

[16] SUGAWARA, S.: Droplet deposition and entrainment modeling based on the three-fluid model. Nuclear Engineering and Design 122, 67–84 (1990).

[17] MARCHIOLI, C., PICCIOTTO, M., SOLDATI, A.: Influence of gravity and lift on particle velocity statistics and transfer rates in turbulent vertical channel flow, International Journal of Multiphase Flow 33 (3), 227–251 (2007).

[18] YAMAMOTO, Y., OKAWA, T.: Effects of particle relaxation time and continuous-phase Reynolds number on particle deposition in vertical turbulent pipe flows, Journal of Nuclear Science and Technology 46 (4), 382–391 (2009).

[19] YAMAMOTO, Y., OKAWA, T.: Effects of particle concentration on particle deposition in turbulent pipe flows, Journal of Nuclear Science and Technology 47 (10), (2010).

[20] OKAWA, T., KITAHARA, T., YOSHIDA, K., MATSUMOTO, T., KATAOKA, I.: New entrainment rate correlation in annular two-phase flow applicable to wide range of flow condition, International Journal of Heat and Mass Transfer 45 (1), 87–98 (2001).

[21] UEDA, T., INOUE, M., NAGATOME, S.: Critical heat flux and droplet entrainment in boiling of falling liquid films, International Journal of Heat and Mass Transfer 24 (7), 1257–1266 (1981).

[22] OKAWA, T., KOTANI, A., KATAOKA, I., NAITO, M.: Prediction of critical heat flux in annular flow using a film flow model, Journal of Nuclear Science and Technology 40 (6), 388-396 (2003).

[23] WALLIS, G. B.: One-dimensional two-phase flow, McGraw-Hill, New York, 315–374 (1969).

[24] UEDA, T., ISAYAMA, Y.: Critical heat flux and exit film flow rate in a flow boiling system, International Journal of Heat and Mass Transfer 24 (7), 1267–1276 (1981).

[25] SUGAWARA, S., MIYAMOTO, Y., FIDAS: Detailed subchannel analysis code based on the three-fluid and three-field model, Nuclear Engineering and Design 120 (2-3), 147–161 (1990).

[26] YOKOBORI, S., OHTA, M., TERASAKA, H., MOROOKA, S.: A phenomenological study on the dryout mechanism in a fuel rod, Proceedings of 4th International Topical Meeting on Nuclear Reactor Thermal-Hydraulics, Karlsruhe, Germany, 1054–1061 (1989).

[27] CHUNG, J. B., BAEK, W.-P., CHANG, S. H.: Effects of the spacer and mixing vanes on critical feat flux for low-pressure water at low-velocities, International Communications in Heat and Mass Transfer 23, 757–765 (1996).

[28] OKAWA, T., KOTANI, A., SHIMADA, N., KATAOKA, I.: Effects of a flow obstacle on the deposition rate of droplets in annular two-phase flow, Journal of Nuclear Science and Technology 41 (9), 871–879 (2004).

[29] OKAWA, T., KOTANI, A., SHIMADA, N., KATAOKA, I.: Measurement of the deposition rate of droplets in a vertical tube containing a flow obstacle, Nuclear Technology 158 (2), 304–313 (2007).

[30] OKAWA, T., FUJITA, T., MINAMITANI, J., KATAOKA, I.: On the deposition rate of droplets in annular flow around a flow obstacle, Multiphase Science and Technology 19 (4), 305–321 (2007).

[31] OKAWA, T., MURAKAMI, T., TAKEI, R.: Measurement of droplet deposition in a small vertical tube, Proceedings of 13th International Topical Meeting on Nuclear Reactor Thermal-Hydraulics, Kanazawa, Japan, Paper No. N13P1075 (2009).

[32] OZAWA, M., Two-phase flow instabilities, in: S. G. Kandlikar, M. Shoji, V. K. Dhir (Eds.): Handbook of phase change: boiling and condensation, Taylor & Francis, Philadelphia, Pennsylvania, 261–278 (1999).

[33] OKAWA, T., GOTO, T., MINAMITANI, J., YAMAGOE, Y.: Liquid film dryout in a boiling channel under flow oscillation conditions, International Journal of Heat and Mass Transfer 52, 3665–3675 (2009).

[34] OKAWA, T., MURAKAMI, T., KATAOKA, I.: A simple model for the dryout heat flux under oscillatory flow conditions, Proceedings of 5th European-Japanese Two-Phase Flow Group Meeting, Spoleto, Italy (2009).

[35] WHITHAM, G. B.: Linear and nonlinear waves, John Wiley & Sons, New York, 19–67 (1999).

[36] HEWITT, G. F., HALL-TAYLOR, N. S.: Annular two-phase flow, Pergamon Press, Oxford, UK, 98–126 (1970).

[37] OKAWA, T., GOTO, T., YAMAGOE, Y.: Liquid film behavior in annular two-phase flow under flow oscillation conditions, International Journal of Heat and Mass Transfer 53, 962–971 (2010).

[38] HALL-TAYLOR, N. S., NEDDERMAN, R. M.: The coalescence of disturbance waves in annular two phase flow, Chemical Engineering and Science 23, 551–564 (1968).

[39] REIN, M.: Phenomena of liquid drop impact on solid and liquid surfaces, Fluid Dynamics Research 12, 61–93 (1993).

[40] OKAWA, T., SHIRAISHI, T., MORI, T.: Production of secondary drops during the single water drop impact onto a plane water surface, Experiments in Fluids 41 (6), 965–974 (2006).

[41] COSSALI, G. E., COGHE, A., MARENGO, M.: The impact of a single drop on a wetted solid surface, Experiments in Fluids 22, 463–472 (1997).

[42] HINZE, J. O.: Turbulence, McGraw-Hill, New York, 451–564 (1959).

[43] OKAWA, T.: More on the droplet deposition in annular two-phase flow, Proceedings of 6th International Conference on Multiphase Flow, Leipzig, Germany, Paper No. KN-8 (2007).

[44] OKAWA, T., SHIRAISHI, T., MORI, T.: Effect of impingement angle on the outcome of single water drop impact onto a plane water surface, Experiments in Fluids 44 (2), 331–339 (2008).

[45] MUNDO, C., SOMMERFELD, M., TROPEA, C.: Droplet-wall collisions: experimental studies of the deformation and breakup process, International Journal of Multiphase Flow 21 (2), 151–173 (1995).

[46] SADATOMI, M., KAWAHARA, A., KANO, K., SUMI, Y.: Single- and two-phase turbulent mixing rate between adjacent subchannels in a vertical 2×3 rod array channel, International Journal of Multiphase Flow 30 (5), 481–498 (2004).

[47] CHUN, T.-H., HWANG, D.-H., BAEK, W. P., CHANG, S. H.: Assessment of a tube-based bundle CHF prediction method using a subchannel code, Annals of Nuclear Energy 25 (14), 1159–1168 (1998).

[48] SAITO, T., HUGHES, E. D., CARBON, M. W., Multi-fluid modeling of annular two-phase flow, Nuclear Engineering and Design 50 (2), 225–271 (1978).

[49] TAMAI, H., KURETA, M., LIU, W., SATO, T., NAKATSUKA, T., OHNUKI, A., AKIMOTO, H.: Effect of rod bowing on critical power based on tight-lattice 37-rod bundle experiments, Journal of Nuclear Science and Technology 45 (6), 567–574 (2008).

[50] HOTTA, A., NOZAKI, K.-I.: Status of thermal-hydraulic performance evaluation of BWR fuels based on subchannel code NASCA, Transactions of the Japan Society of Mechanical Engineers, Part B 76 (763), 454–456 (2010).